Emerging Coherence of Oscillating Chemical Reactions on Arrays: Experiments and Simulations

Yumei Zhai, István Z. Kiss, and John L. Hudson*

Department of Chemical Engineering, University of Virginia, 102 Engineers' Way, Charlottesville, Virginia 22904-4741

We report experiments on emerging coherence through weak global coupling of populations of electrochemical oscillators with heterogeneities. The experiments are done with an array of nickel electrodes undergoing electrodissolution in sulfuric acid. The experiments verify theories of Winfree and Kuramoto that predict that global coupling of a set of smooth limit cycle oscillators with different frequencies produces a phase transition in which some of the elements synchronize. Both the critical point and the predicted dependence of order on coupling are seen in the experiments. We extend the studies to relaxation oscillators and characterize the quantitative similarities and differences between the two types of systems. Numerical simulations using a coupled form of a nickel electrodissolution model support the experimental findings.

Introduction

A distributed chemically reacting system can often be thought of as an ensemble of reacting sites. The spatiotemporal variations of the local and mean reaction rates depend on kinetics of individual reacting sites and the strength and length scale of the interactions among them. A number of spatiotemporal pattern types have been observed in reaction−diffusion systems in which the coupling is local.[1] In heterogeneous chemical reactions, long-range and global interactions should also be considered. Global coupling in gas−solid systems is imposed by mixing in the gas phase because a consumption of reactants or production of products at one location causes changes in conditions at all locations.[2−4] Constraints such as temperature control can also result in global coupling.[5] In electrochemical systems, the coupling is typically long-range;[6] the reacting sites interact at a length scale depending on cell geometry through the potential drop in the electrolyte.[7] Global coupling occurs in electrochemical systems in the galvanostatic (constant-current) mode of operation as a result of the imposed constraint.[8] A series resistor in the potentiostatic mode has a similar global coupling effect;[6,8,9] changes of currents of one reacting site change the resistor potential drop, which influences the potential of all locations.

Global coupling in these systems can have important effects on both local dynamics and pattern formation. Strong global coupling of periodic sites in the modified Ginzburg−Landau equation[2] and in a model of CO oxidation on Pt(110)[10] leads to synchronization, turbulence, and standing-wave oscillations. Global interactions enable the formation of patterns in cases where the interaction between local diffusion and reaction alone cannot cause pattern evolution.[11] A rich variety of patterns such as circular- or stripe-shaped regions of activity were found on ring, ribbon, and disk catalysts.[4,11] Dynamical differentiation, or clustering, was recently observed in globally coupled chaotic and periodic metal electrodissolution.[12,13]

Heterogeneity or nonuniformity is ubiquitous in surface reaction systems. The heterogeneity arises as a result of variations in the local surface and/or transport properties. It may develop in the course of an experiment by some symmetry-breaking pretreatment, or it may be due to a variation of the local density of the catalyst, porosity, catalyst thickness, nonuniformities of the temperature distribution in the reactor, or imperfect mixing in the fluid phase (see ref 14 and references therein). Heterogeneities play the role of nucleation centers and induce the collapse of long-range order in solid−gas-phase reactions.[2] Novel patterns can arise in systems with heterogeneities; an example is a rotating pulse on a ring that can rotate in one direction but not in the other.[15] Nonuniformity can increase the number of possible patterns and also affects the sensitivity of patterns to changes in initial conditions or perturbations.[15]

Even very weak coupling among sites can have significant effects on the collective dynamics of a system.[1,16−18] Consider a system with small heterogeneities that produce a frequency distribution of a set of oscillating reacting sites.[3,12,14,19] A weak global coupling has small quantitative effects, but no qualitative effects, on the local dynamics but can influence the collective or spatially averaged dynamics.[14,17,18] In chemically reacting systems, the spatially averaged reaction rate is often the quantity of interest because it gives the overall conversion in the reactor.

With weak coupling, an important question is the emergence of coherence of the individual elements. Synchronization theories of Winfree and Kuramoto have played a fundamental role in the development of the field of nonlinear science dealing with collective dynamics.[1,16] In their work a population of an infinite number of ideal oscillators is considered. Each oscillator is described by only one variable, the phase, and changes of the amplitudes are not considered. The weak coupling affects the frequencies of the population of oscillators.[16] Winfree has shown that there exists a critical coupling strength at which the oscillators begin to synchronize and a coherent mean-field solution emerges.[20] Kuramoto developed an elegant mean-field analysis and gave analytical solutions for the order (e.g., number of synchronized oscillators) as a function of coupling strengths for smooth oscillators.[1,21,22] These results

* To whom correspondence should be addressed. Tel.: 434-9246275. Fax: 434-9822658. E-mail: hudson@virginia.edu.

10.1021/ie030164z CCC: $27.50 © 2004 American Chemical Society
Published on Web 07/10/2003

initiated extensive theoretical activity in collective dynamics and extensions to the effects of finite-size populations,[23] of fluctuations,[1] and of more complicated waveforms and coupling mechanisms.[24,25] Strogatz has reviewed recent advances.[26] Engineering applications include microwave communications,[27] high-power laser devices,[28] and superconducting electronic systems.[29] Visual and audio interactions make crickets chirp,[30] fireflies flash,[31] and audiences clap[32] in synchrony. Mutual synchronization has been shown to be important in interpreting glycolitic oscillations,[33−35] α rhythms in the brain,[36] and aggregate beating of heart cells.[16,37]

Although emerging coherence has importance in many systems, for diverse technical reasons, the systems have not lent themselves to the quantitative observations needed to test the theory.[38] In this paper we present results of laboratory experiments with populations of globally coupled electrochemical oscillators. The experimental system consists of an array of periodically dissolving nickel electrodes.[12] The current on each electrode can be individually measured, and global coupling can be applied with a combination of series and parallel resistors. We investigate the phase transition and dependence of order on coupling strength predicted by the theory on smooth limit cycle oscillators[21] and the enhancement of fluctuations near the critical point that arise in finite-size systems.[23] In addition, we extend the experiments to relaxation oscillators that often occur in physical and biological systems. We investigate the onset of coherence, the dependence of order, and finite-size fluctuations on the coupling strength and compare the characteristics of the two types of oscillators. (A brief account of a portion of the experimental results can be found in a recently published paper.[39]) The experimental findings are supported by numerical simulations with a globally coupled electrochemical model describing the dissolution of nickel in sulfuric acid.

Experiments: Apparatus and Procedure

The experimental system used for the study is an array of 64 nickel electrodes in an 8 × 8 geometry. The array was placed in a 3 mol/L sulfuric acid electrolyte at 11 °C. Nickel dissolution on the surface of the electrode occurred at an applied potential (V vs Hg/Hg_2SO_4/saturated K_2SO_4 reference electrode) held constant by a potentiostat. A schematic of the experimental apparatus and its description are given in a recent publication.[17] The current, proportional to the rate of reaction, was measured at a sampling rate of 100 Hz on each electrode to provide dynamical information of the elements of the population. Zero-resistance ammeters were used to convert each individual current into a potential that was recorded by a transputer (Adwin Pro, Keithley). Testpoint software was used to visualize and save the data. The electrolyte was stirred with a magnetic stirrer at a speed of 250 rpm. The electrodes are 1 mm in diameter and are equally spaced with 2 mm; it has been shown that the short-range coupling through the effect of stirring can be ignored with this spacing.[17]

The electrodes were connected to the potentiostat through one series (collective) resistor (R_s) and through N parallel (individual) resistors (R_p), where N is the number of electrodes. Heterogeneity due to variations in the surface of the electrodes and transport always exists in the experiments and causes a frequency distribution in the individual oscillating currents.[12] In addition, we used small random resistors (with a standard deviation of 21 Ω) to increase the variance of the frequency distribution; experiments without these resistors gave similar results to those shown but with a slight loss in reproducibility. Mean parallel resistors in the range of 400−650 Ω were used in the studies of smooth and relaxation oscillators.

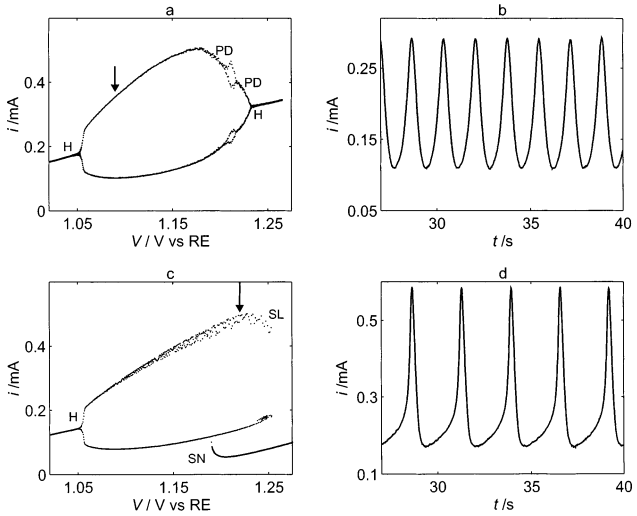

Figure 1. Experiments: single oscillator. Top row: smooth oscillator. (a) Polarization curve at R_{tot} = 7.1 Ω and scan rate = 0.2 mV/s. For periodic current, only maxima and minima are shown. (b) Current time series at V = 1.09 V (indicated by the arrow in panel a). Bottom row: relaxation oscillator. (c) Polarization curve at R_{tot} = 10.2 Ω, and scan rate = 0.2 mV/s. (d) Current time series at V = 1.22 V (indicated by the arrow in panel c). H, PD, SN, and SL are Hopf, period doubling, saddle-node, and saddle-loop bifurcations, respectively.

The collective resistor couples the electrodes globally.[12,13] To study the effect of various global coupling strengths on the behavior of the system, we held the total external resistance (R_{tot}) constant while the fraction dedicated to individual currents, as opposed to the total current, was varied. Thus, all other parameters of the system are constant (i.e., the kinetics and the parameters of the individual oscillators are not changed) while the strength of global coupling can be varied. A global coupling parameter K is defined as

$$K = \frac{R_s/R_{tot}}{1 - R_s/R_{tot}} \qquad (1)$$

The total resistance is $R_{tot} = R_s + R_p/64$, where R_p is the mean parallel resistor. For $K = 0$, the external resistance furnishes no additional global coupling; for $K = \infty$, maximal external global coupling is achieved.

Experimental Results

A. Single Electrode. The electrodissolution of nickel in sulfuric acid is oscillatory in appropriate ranges of the parameters: applied potential, acid concentration, and added external resistance.[12,40] Figure 1a shows the current as a function of the applied potential for a small external resistance. (The experiment is done at a low scan rate; the dynamics at a series of constant potentials are essentially the same as those shown.) Below V = 1.053 V and above 1.233 V, the current is steady. Between these two values, oscillations occur; in this region the maxima and minima of the current oscilla-

tions are shown. A Hopf bifurcation occurs at about $V = 1.053$ V, above which current oscillations develop. A representative time series showing nearly sinusoidal oscillations of current at constant potential is shown in Figure 1b. The angular velocity (in state space, see Figure 2a) is almost constant, although there is a slight slowing down at minimum values of the current; we refer to these oscillations as smooth. Except for a small region of period doubling (1.205 V $< V <$ 1.216 V), the oscillations keep their smooth character for a wide region of circuit potential. The oscillations cease with another Hopf bifurcation at about $V = 1.233$ V.

At larger resistance, the bifurcation structure (Figure 1c) is more complicated and the smooth oscillations do not dominate the whole oscillatory region. The oscillations set in at a Hopf bifurcation at about $V = 1.051$ V, and they keep their smooth character up to about $V =$ 1.15 V. The oscillations cease at $V = 1.253$ V with a saddle-loop bifurcation. Below the saddle-loop bifurcation, there is a region of relaxation oscillations where the angular velocity varies with time. The periods of the relaxation oscillators are usually longer than those of the smooth oscillators. More detailed discussions of the dynamics of the nickel−sulfuric acid system can be found in a recent review;[6] the system belongs to the class of HNDR (hidden negative differential resistance) oscillators.

In this study we discuss the onset of synchronization of globally coupled populations of both smooth and relaxation oscillators.

B. Arrays of Smooth Oscillators. Results obtained with an array of 64 periodic smooth oscillators without added global coupling ($K = 0$) are shown in Figure 2. The limit cycle for one of the oscillators is presented in Figure 2a. We used the Hilbert transform $H[i(t) - \langle i\rangle]$, where $i(t)$ is the current and $\langle i\rangle$ is its temporal mean, to construct the phase space and to obtain the phase of an individual oscillator.[41,42] The Hilbert transform is defined as

$$H[i(t) - \langle i\rangle] = 1/\pi \int_{-\infty}^{\infty} \frac{i(\tau) - \langle i\rangle}{t - \tau}\, d\tau \qquad (2)$$

The phase at time t is obtained as the angle (ϕ) in Figure 1a, i.e.,

$$\phi(t) = \arctan \frac{H[i(t) - \langle i\rangle]}{i(t) - \langle i\rangle} \qquad (3)$$

The phase as a function of time is shown in Figure 2b; for this smooth oscillator, it is nearly a linear function of time. The frequency of the oscillator is then obtained from the slope. The use of the Hilbert transform in constructing the state-space representation and the phase and frequency has been discussed.[17]

The frequencies of the 64 oscillators without added global coupling are shown in Figure 2c. The points on a snapshot in $H[i(t) - \langle i\rangle]$ vs $i(t) - \langle i\rangle$ space for the 64 oscillators are well distributed on the limit cycle (Figure 2d); this indicates a lack of coherence.

Experimental results obtained at three values of the coupling parameter are shown in Figure 3. The dimensionless frequency distribution without added coupling ($K = 0$) is shown in Figure 3a. (There is a slow drift in the experiments toward smaller frequencies; therefore, before each experiment the frequencies at $K = 0$ were measured and used to normalize the frequencies of the subsequent experiment.) The frequencies in Figure 3a

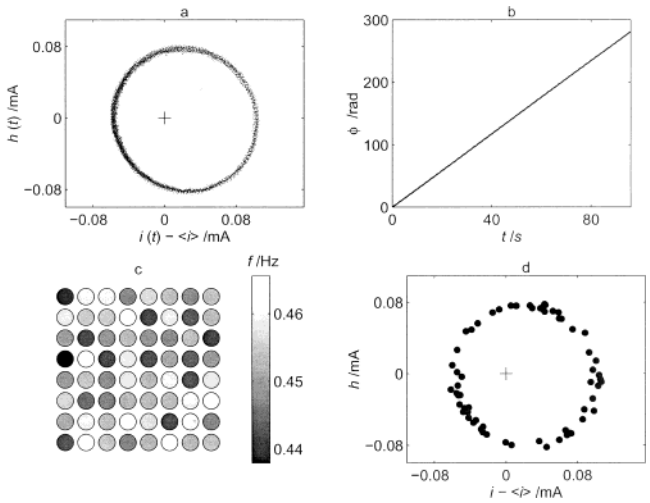

Figure 2. Experiments: phase portraits, phase, and frequencies of the 64 uncoupled smooth oscillators. (a) Phase portrait of a single oscillator obtained with a Hilbert transform. (b) Phase of a single oscillator vs time. (c) Intrinsic frequencies of the 64 array of smooth oscillators. (d) Snapshot of the 64 oscillators in the phase space.

correspond to those seen in Figure 2c on the array. Inherent heterogeneities produce a distribution of frequencies of the oscillators; as noted above, we have added random resistors, which increased the spread of this distribution and smoothed it somewhat by choosing a distribution of parallel external resistors. The frequency distribution is approximately unimodal with a mean of 0.4526 Hz and a standard deviation of 6.54 mHz.

The frequency distributions at two nonzero values of K are shown in parts b and c of Figure 3. It can be seen from a comparison of parts a and b of Figure 3 that a small amount of coupling induces synchronization of the oscillators having a frequency near the mean but that the oscillators with frequencies farther from the mean are not significantly affected. An additional increase in the coupling strength, Figure 3c, leads to a phase synchronization of all of the oscillators. Thus, the effect of adding small amounts of coupling is to bring a few of the elements having frequencies near the mean to some common frequency. As the coupling is increased, the number of elements in the phase-synchronized group increases. Finally, all of the oscillators obtain the same frequency.

This effect can also be seen in parts d−f of Figure 3, where the oscillator frequencies as functions of their natural frequencies are shown for the same three values of coupling strength. For $K = 0$, deviations from the 45° line are small. (Any deviation is simply an indication of experimental error as the data for the abscissa and ordinate were taken from two experiments at the same parameter values.) We see from Figure 3e that the oscillators with frequencies near the mean become coherent as the coupling is increased but those far above and far below the mean remain unsynchronized; for K greater than approximately 0.085, all of the oscillators have the same frequency and fall on the horizontal line.

An order parameter $r(t)$, defined as the normalized length of the vector sum of the phase points [$\mathbf{P}_j(t)$] in Figure 2d, is a measure of coherence:

$$r(t) = |\sum_j \mathbf{P}_j(t)| / \sum_j |\mathbf{P}_j(t)| \qquad (4)$$

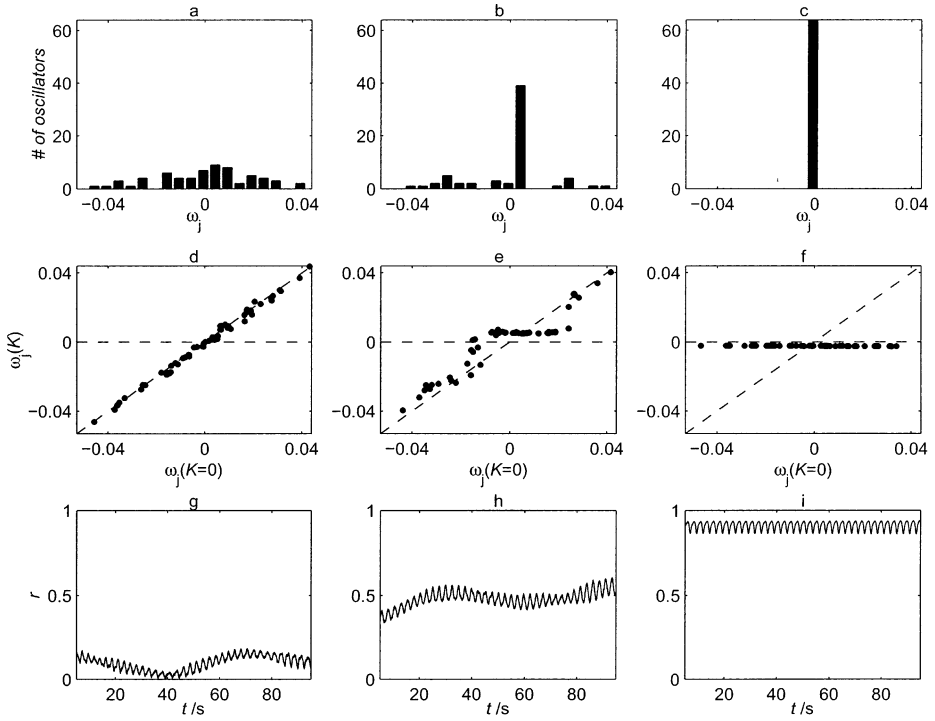

Figure 3. Experiments: 64 array of smooth oscillators at $V = 1.075$ V, $R_{tot} = 10.2\ \Omega$, and $K_c = 0.03$. Left column: $K = 0$. Middle column: $K = 0.035$. Right column: $K = 0.085$. Top row: histograms of the dimensionless frequencies $\omega_j = f_j/\langle f_0\rangle - 1$, where $\langle f_0\rangle$ is the mean frequency of oscillators at $K = 0$. Middle row: dimensionless frequencies at different coupling strengths $\omega_j(K)$ versus the corresponding frequencies without coupling ($K = 0$). The horizontal dashed line ($\omega_j = 0$) represents the mean intrinsic frequency. The diagonal dashed line [$\omega_j(K=0)$] corresponds to intrinsic frequencies. Bottom row: time series of the order parameter.

This parameter is similar to that introduced by Kuramoto in his study of coupled phase oscillators;[1] the order parameter has a value of 1 when the points are exactly synchronized and of 0 for an uncorrelated infinite set of ideal smooth oscillators. For a finite-size system, the mean value of the order is greater than 0 even without coupling. A series of experiments with increasing number of oscillators ($N = 2, 4, ..., 64$) showed that the mean order is proportional to $1/\sqrt{N}$ (see Figure 4a); in these experiments $\langle r\rangle \approx 1/\sqrt{N}$. The order parameter as a function of time is shown in Figure 3g for the uncoupled set of 64 oscillators and in Figure 3h,i with coupling.

A mean order parameter $\langle r\rangle$, obtained by integrating over time, is shown in Figure 4b as a function of coupling strength. In the theory for an infinite set of oscillators, the order is constant and has a value of 0 for $K < K_c$, where K_c is a critical point.[1] The order in the experiment is approximately independent of coupling for small values of K; $\langle r\rangle$ is nonzero, but small, because of the finite system size. The phase transition can be seen in Figure 4b at $K = K_c = 0.03$. Above 0.03, $\langle r\rangle$ increased sharply with K and additional oscillators become synchronized. At larger K, the mean order parameter $\langle r\rangle$ approaches 1. Kuramoto has shown analytically,[1] for an infinite set of oscillators with a Lorentzian frequency distribution, that $\langle r\rangle$ depends on K above K_c as

$$\langle r\rangle = \sqrt{1 - \frac{K_c}{K}} \qquad (5)$$

For a quantitative comparison with theory, we rescaled the order parameter r to take into account the finite-size character of the system. At low coupling strength, the order in the experiments is nonzero because of the finite size. At large coupling strength, the experimental order can be larger than the theoretical one because there is a finite range of the frequency distribution; thus, the (order-decreasing) contributions of elements at very large and very low frequencies, which would require even larger K for entrainment, are not present.

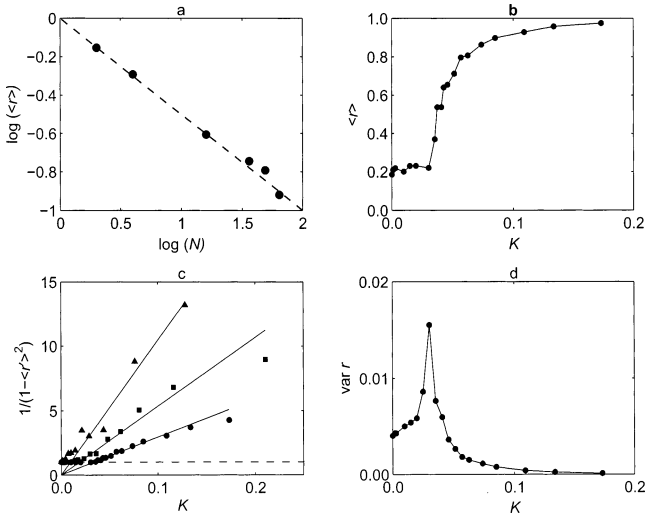

Figure 4. Experiments: 64 array of smooth oscillators. (a) Dependence of the mean order parameter on the number of elements (N). $V = 1.075$ V and $R_{tot} = 10.2\ \Omega$. (b) The mean order parameter as a function of the coupling strength, with the same conditions as those in part a. (c) Dependence of $1/(1 - \langle r'\rangle^2)$ on the coupling strength under different experimental conditions. Triangles: $V = 1.09$ V, $R_{tot} = 7.1\ \Omega$, and $K_c = 0.01$. Squares: $V = 1.085$ V, $R_{tot} = 8.6\ \Omega$, and $K_c = 0.02$. Circles: $V = 1.075$ V, $R_{tot} = 10.2\ \Omega$, and $K_c = 0.03$. Dashed line: $1/(1 - \langle r'\rangle^2) = 1$. (d) Variance of the order parameter as a function of K, with the same experimental conditions as those in part a.

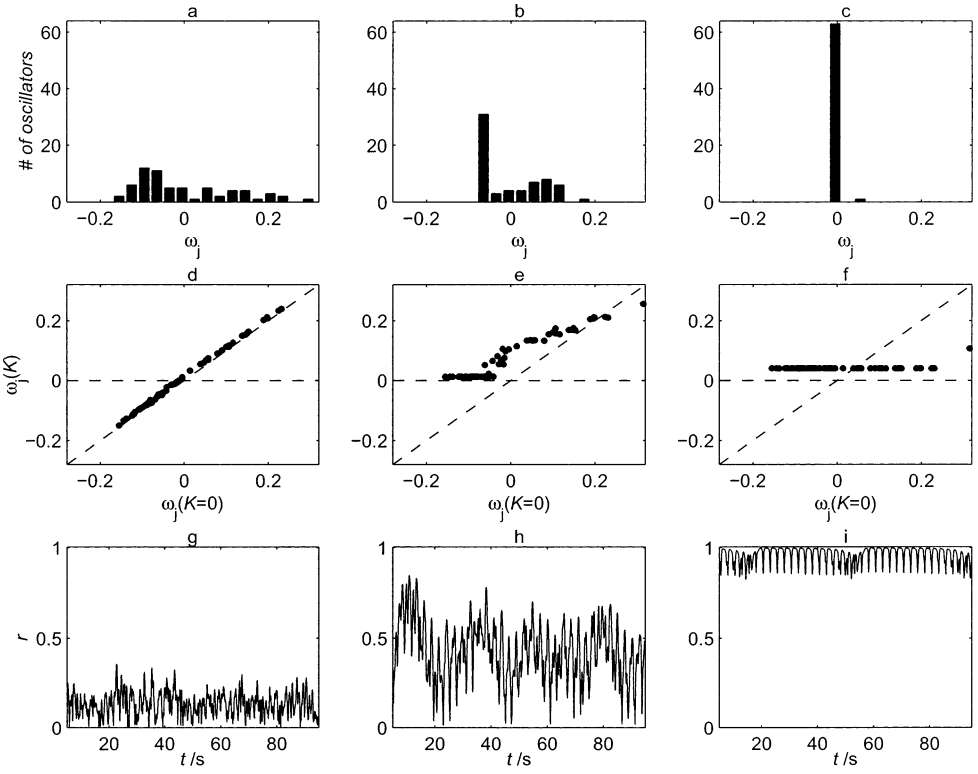

Figure 5. Experiments: 64 array of relaxation oscillators at $V = 1.22$ V, $R_{tot} = 10.2\ \Omega$, and $K_c = 0.23$. Left column: $K = 0$. Middle column: $K = 0.29$. Right column: $K = 0.52$. Top row: histograms of the dimensionless frequencies ω_j. Middle row: dimensionless frequencies at different coupling strengths $\omega_j(K)$ versus the corresponding frequencies without coupling ($K = 0$). Bottom row: time series of the order parameter.

Therefore, a rescaled order r' is defined as

$$r'(t) = \frac{r(t) - r_0}{1 + \delta - r_0} \tag{6}$$

where $r_0 = 1/\sqrt{N}$ is the order at $K = 0$ and δ is a small empirical factor, here 0.05, that takes account of the finite frequency range.

The dependence of $\langle r' \rangle$ on K is shown in Figure 4c for three different sets of experimental conditions. The experimental results are in accordance with the theoretical prediction. Below K_c, the quantity $1/(1 - r'^2)$ is 1, and above K_c, it increases linearly with K with a slope of $1/K_c$.

The order parameter varies with time in the experiments, as was seen in Figure 3. Theoretical and numerical studies of Daido[23] have shown that for finite-size systems the order varies with time and enhanced fluctuations can be observed around the critical point: the variance of r scales with $|K - K_c|^{\alpha}$, where scaling parameter α is -1 for $K < K_c$ and $-1/4$ for $K > K_c$. In the experiments, the variance of r (Figure 4d) has a maximum at K_c consistent with theory. The order often undergoes large changes with time near $K = K_c$; for example, we have seen transitions from an almost unsynchronized behavior at $r = 0.3$ to an almost synchronized state at $r = 0.8$ in some experiments within a time frame of 20 oscillations.

C. Arrays of Relaxation Oscillators. We carried out the same types of experiments at somewhat different experimental conditions where periodic relaxation oscillations are obtained; an example of the waveform was shown in Figure 1d. The frequency distribution ($\langle f_j \rangle = 0.35$ Hz; standard deviation = 39 mHz) of the array of 64 oscillators without added coupling is shown in Figure 5a; it is flatter and broader than that of the smooth oscillators considered above. There is, however, a slight maximum at lower frequency values. As coupling strength K is increased, we see a behavior that is qualitatively similar to that of the smooth oscillators. There is again a critical coupling point K_c at which the onset of synchronization is observed. (The value of K_c becomes larger as the saddle-loop bifurcation is approached through a change of parameters; in this region the relaxation nature of the oscillations is more pronounced.) In Figure 5b,e, obtained just above the critical coupling point, it is seen that the onset of synchronization occurs with the lower frequency oscillators, that is, in the region of the small maximum in the initial frequency distribution. Note that the frequencies of the unsynchronized elements are also affected; there is a shift to higher frequencies. The synchronized region then grows as K is increased until the entire set is synchronized. In contrast to the smooth oscillators, the synchronized frequency is somewhat higher than the mean frequency (see Figure 5c,f).

The order parameter as a function of time is seen in Figure 5g−i. It can be noted that the variation is greater than that seen in the smooth oscillators; the variation is particularly large in Figure 5h, which was obtained with a value of K just above K_c. The intermittent irregular variations of order in Figure 5i are due to occasional phase slips of the single nonentrained element in the population (as seen in Figure 5c,f). The mean order parameter is shown in Figure 6a for two sets of experimental conditions. In general, the critical coupling K_c is larger ($K_c > 0.1$) than that for the smooth oscillators; the increase of order above K_c is very steep. At a potential closer to the saddle−loop bifurcation, K_c is large ($K_c = 0.4$). At coupling strengths greater than

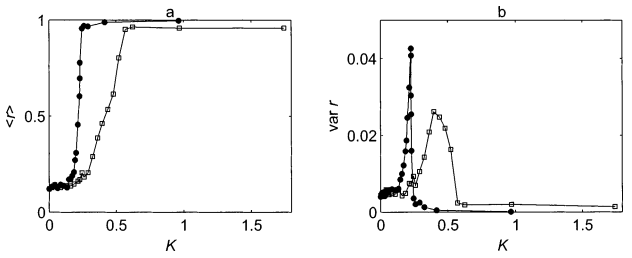

Figure 6. Experiments: 64 array of relaxation oscillators. (a) The mean order parameter as a function of the coupling strength. (b) Variance of the order parameter as a function of K. Solid circles: $V = 1.22$ V, $R_{tot} = 10.2\ \Omega$, and $K_c = 0.23$. Open squares: $V = 1.24$ V, $R_{tot} = 10.2\ \Omega$, and $K_c = 0.4$.

approximately $K = 0.5$, the coupling is no longer weak; changes in the shape of individual oscillators and even partial amplitude clustering can occur.[12] The order in Figure 6a (squares) does not go to 1 because of some period-two characteristics of the oscillations; it does go to 1 at very large coupling strengths where identical synchronization of the elements occurs and the individual shapes of the oscillators are again similar to those of the uncoupled case.

The plots of var r vs K (Figure 6b) show enhanced fluctuations around K_c similar to those found with smooth oscillators; however, the magnitude of var r at K_c is larger than that obtained for smooth oscillators and seen in Figure 4.

Simulation Results

A. Model. To confirm the experimental findings, to interpret the transitions, and to obtain additional information on the dependence of emerging coherence on types of oscillators, system size, and frequency distributions, numerical simulations were carried out. We used a model of anodic electrodissolution of a single nickel electrode proposed by Haim et al.[43] The model in a dimensionless form involves two variables: the dimensionless double-layer potential drop (e) and the surface coverage of NiO + NiOH (θ). One oscillator is described by the following two equations:

$$\frac{de}{dt} = \frac{V - e}{R} - i_F(\theta,e) \tag{7}$$

$$\Gamma \frac{d\theta}{dt} = \frac{\exp(0.5e)}{1 + C_h \exp(e)}(1 - \theta) - \frac{bC_h \exp(2e)}{cC_h + \exp(e)}\theta \tag{8}$$

where V is the dimensionless applied potential, R is the dimensionless series resistance, Γ is the surface capacity, and i_F is the Faradaic current:

$$i_F = \left[\frac{C_h \exp(0.5e)}{1 + C_h \exp(e)} + a \exp(e)\right](1 - \theta) \tag{9}$$

Equation 7 is for the charge balance in the equivalent circuit of the electrochemical reaction; eq 8 is from the simplified mass balance and kinetics. The current of an electrode is calculated as $i(t) = [V - e(t)]/R$. The parameter values $C_h = 1600$, $a = 0.3$, $b = 6 \times 10^{-5}$, and $c = 1 \times 10^{-3}$ were optimized[43] to obtain dynamical features similar to experiments.

Bifurcation diagrams and some typical oscillation waveforms are presented in Figure 7. In Figure 7a the variable e is shown as a function of circuit potential V for a relatively low value of resistance, $R = 5.4$. As in the experimental results (Figure 1a), the oscillations develop and cease through Hopf bifurcations. Time series of e and i (Figure 7b,c) show the smooth nature of the oscillations under these conditions. At larger resistance ($R = 20$), the oscillations again arise through a Hopf bifurcation, as seen in the bifurcation diagram in Figure 7d; however, they cease through a saddle-loop bifurcation at $V = 26.5$. As the saddle-loop bifurcation is approached, relaxation oscillations are observed and the oscillation period becomes larger (Figure 7e,f). The dynamical features of the model in parameter regions shown in Figure 7 are very similar to those seen in the experiments (Figure 1). Therefore, we shall use these parameters to simulate the experimental results of the smooth and relaxation oscillators.

A model of the population of globally coupled nonidentical oscillators is developed in two steps. First, the nonidentical character of the individual oscillators is defined. Second, the equation for coupling through the collective (series) resistance is derived.

In the experiments the oscillators are inherently different because of heterogeneities[12] and because of the different individual resistors. We model the nonidentical nature of the oscillators by giving the oscillators different values for the parameters R and Γ in eqs 7 and 8. (Other choices are also possible; however, these parameters seem to be the most reasonable ones.) For element k, the resistance and the surface capacitance are obtained using the relationships $R_k = (1 + \Delta_k)R0$ and $\Gamma_k = (1 + \Delta_k)\Gamma 0$, where Δ_k is a heterogeneity parameter and $R0$ and $\Gamma 0$ are the mean values. We used a fixed value of $\Gamma 0 = 0.01$ throughout this paper. Thus, if $\Delta_k = 0.05$, the electrode has parameter values 5% larger than the mean value. The frequency of the oscillator varies almost linearly in Δ_k in most parameter regions (except very close to the saddle-loop bifurcations; see below) if the value of Δ_k is small. Given a certain narrow distribution of Δ_k, the frequency of a population of (uncoupled) oscillators described by eqs 7 and 8 will follow the same distribution. We choose either a Lorentzian or Gaussian distribution for Δ_k. Most simulations we shall discuss were done with a Lorentzian distribution because the analytical solutions from Kuramoto's theory[1] are easily obtained for this distribution. However, for comparison, simulations were also made with a Gaussian distribution. The Lorentzian distribution $[p(x) = \gamma/\{\pi[(x - x_0)^2 + \gamma^2]\}]$ is characterized by a parameter γ; 2γ is the half-width of the distribution. For a typical value of $\gamma = 0.5$, the equation parameters R_k and Γ_k vary within a range of 5% of their means.

Global coupling is added to the elements through resistors. Because the coupling is electrical, it only appears in the equation for the variable e. The model for the coupled set of N oscillators is then

$$\frac{de_k}{dt} = \frac{V - e_k}{R_k} - i_{F,k}(\theta_k,e_k) + \frac{1}{R0}K(e_{mean} - e_k) \tag{10}$$

$$\Gamma_k \frac{d\theta_k}{dt} = \frac{\exp(0.5e_k)}{1 + C_h \exp(e_k)}(1 - \theta_k) - \frac{bC_h \exp(2e_k)}{cC_h + \exp(e_k)}\theta_k \tag{11}$$

where $k = 1, ..., N$, $e_{mean} = (1/N)\Sigma e_k$ is the mean potential drop, and K is the same coupling parameter as that used in the experiments (see eq 1). The last term in eq 10 that produces the coupling among the oscillators was obtained from an analysis of a simple equivalent circuit

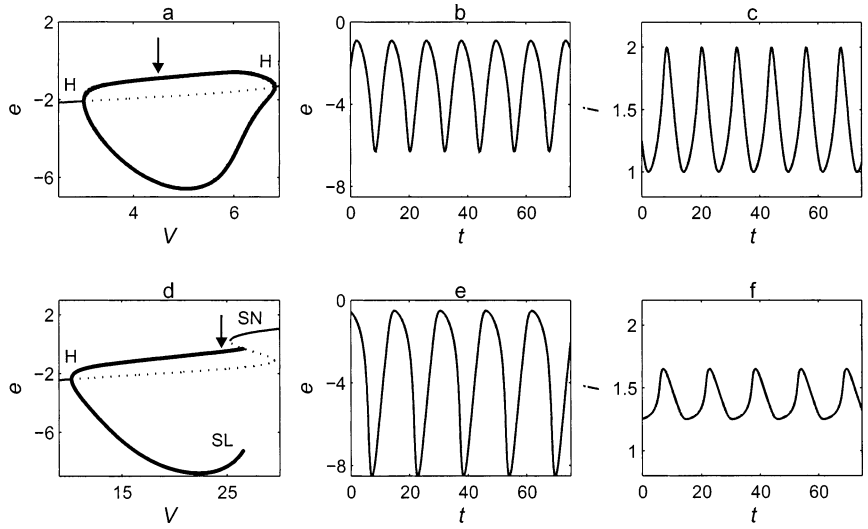

Figure 7. Simulations: single oscillator. Top row: smooth oscillator. (a) One parameter bifurcation diagram at $R0 = 5.4$. Solid thin line: stable steady state. Dotted line: unstable steady state. Solid thick line: maxima and minima of periodic solutions. (b) Time series of the calculated potential drop through the double layer at $V = 4.5$ (indicated by the arrow in panel a). (c) Time series of the calculated current at $V = 4.5$. Bottom row: relaxation oscillator. (d) One parameter bifurcation diagram at $R0 = 20$. The types of lines have the same explanations as those in part a. (e) Time series of the calculated potential drop through the double layer at $V = 24.5$ (indicated by the arrow in panel d). (f) Time series of the calculated current at $V = 24.5$. H, SN, and SL are Hopf, saddle-node, and saddle-loop bifurcations, respectively.

of the system[44] with the assumption that $\Delta_k \ll 1$. (The equations are exact for two oscillators but approximate for larger values of N.) $K = 0$ represents uncoupled oscillators; $K \rightarrow \infty$ yields maximum global coupling that synchronizes the oscillators. A variable-step-size fourth-order Runge−Kutta method of Matlab was used to integrate eqs 10 and 11 with a display step size of $\Delta t = 0.5$, absolute error $= 10^{-6}$, and relative error $= 10^{-3}$. Smaller step sizes and error limits gave the same results. A transient of $t = 10\,000$ was discarded from each time series. The mean and variance of order are averages of three runs with different initial conditions. The phases and frequencies of simulated oscillators are determined from time series data of $e_k(t)$.

B. Arrays of Smooth Oscillators. We begin with simulation results of 64 globally coupled smooth oscillators with a Lorentzian distribution in Δ_k. A typical condition for a population of smooth oscillators is $V = 4.5$, $R0 = 5.4$, and $\gamma = 0.5$. Figure 8 shows the frequency distributions and time series of order parameters with different coupling strengths K under this condition. We can see that, without coupling (first column in Figure 8), the intrinsic frequency distribution is approximately unimodal and symmetric. The spread of the frequencies is of similar order of magnitude as that of the experiments; the fastest and slowest oscillators have frequencies 2.5% larger and smaller than the mean, respectively. In the experiments this value is about 4% (see Figure 3). The order parameter of this population without coupling (Figure 8g) fluctuates around 0.11; in the simulations, as in the experiments, the mean order parameter without coupling is close to $1/\sqrt{N}$, or $^1/_8$. The second and third columns in Figure 8 show the behavior with small, but increasing, added coupling. At $K = 0.022$, oscillators with intrinsic frequencies slightly smaller than the mean are synchronized and those far away from the mean are unaffected except for a small shift to higher frequencies (Figure 8b,e). The shift to higher frequencies and the tendency for elements with frequencies slightly below the mean to synchronize first are seen generally in the simulations. These effects are small with smooth oscillators but are much stronger with relaxation oscillators, as we shall see below. As seen in Figure 8h, the mean order parameter increases to about 0.38 because of the increased synchrony among the elements; the variations in the order are also larger than those at smaller coupling. With further increases in the coupling strength, more and more elements join the synchronized group of elements. The synchronized frequency gets closer to the mean of the natural frequencies. With larger coupling ($K = 0.16$, third column), all of the elements have a frequency of the mean of their intrinsic frequencies. The order parameter reaches a large mean value of about 0.99 and has only small variations.

The mean order parameter as a function of coupling strength is shown in Figure 9a. The nonzero mean order at $K = 0$ is due to the finite size of the sample. At low values of K, the order increases slowly with increasing K; this is followed by a steeper increase. Figure 9b shows the relationship between the rescaled order parameter as a function of K at three different conditions that yield different critical coupling strengths. The variation of order with K can be interpreted in the framework of Kuramoto's theory for all three conditions. (All K_c values are obtained by taking the reciprocal of the slope of the fitting lines.)

The variance of order as a function of coupling strength is shown in Figure 9c,d for two different conditions. The conditions in Figure 9c are the same as those for Figure 9a. Enhanced fluctuations of the order parameter near the critical point can be observed. Near the critical point, two peaks can be seen. The first peak occurs approximately at the coupling strength at which oscillators with frequencies smaller than the mean are synchronized. The second peak occurs at a coupling strength just below the value at which elements with frequencies higher than the mean start to synchronize. The oscillators with lower frequencies are easier to entrain, and thus the synchronization occurs in two steps in a small region of coupling strength. Figure 9d shows the variance of order vs K for a population with a narrower intrinsic frequency distribution and thus a smaller K_c. When the frequency difference among the

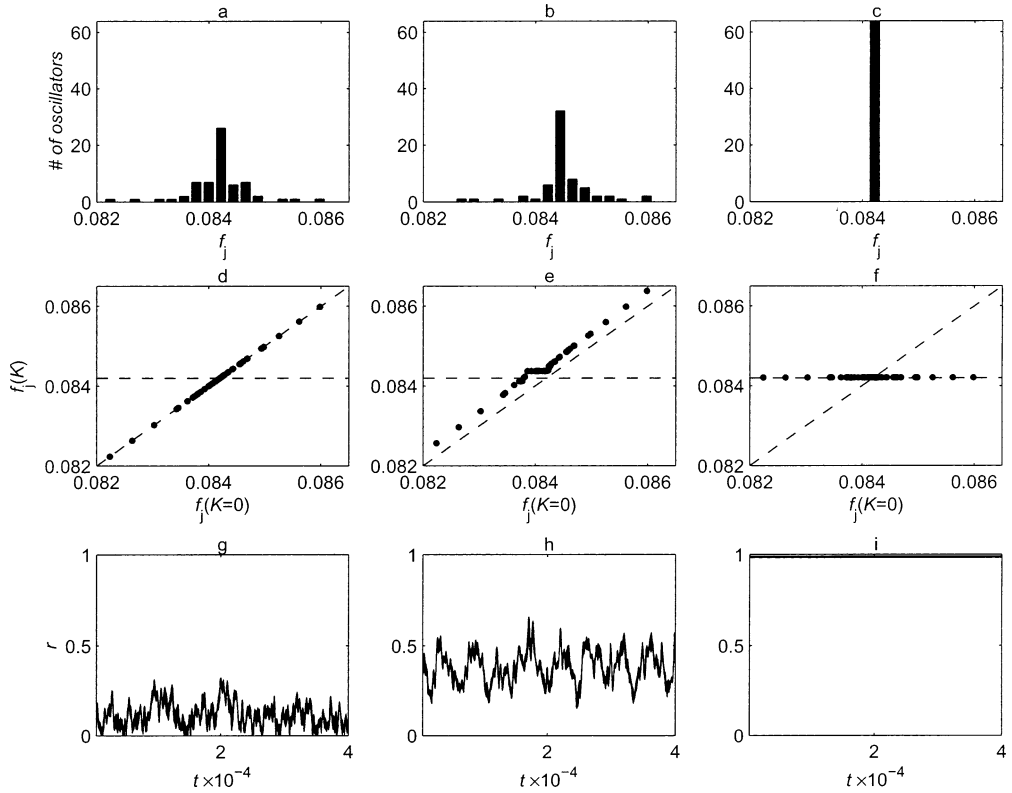

Figure 8. Simulations: 64 globally coupled smooth oscillators at $V = 4.5$, $R0 = 5.4$, $\gamma = 0.5$, and $K_c = 0.021$. Left column: $K = 0$. Middle column: $K = 0.022$. Right column: $K = 0.16$. Top row: histograms of the frequencies f_j. Middle row: frequencies at different coupling strengths $f_j(K)$ versus the corresponding frequencies without coupling ($K = 0$). Horizontal dashed line: the mean intrinsic frequency. Diagonal dashed line: intrinsic frequencies. Bottom row: time series of the order parameter.

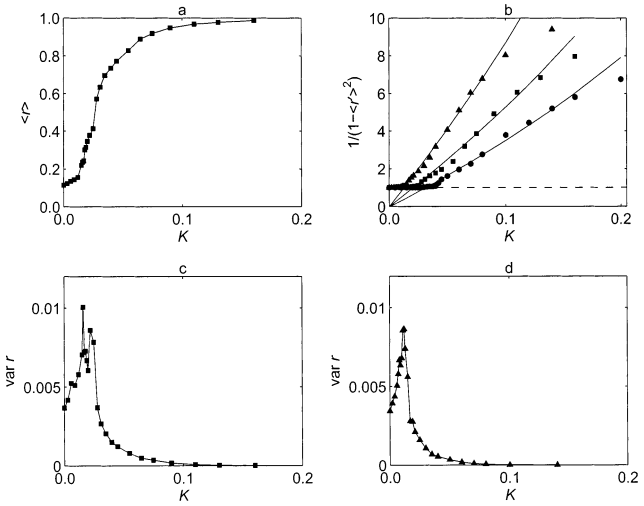

Figure 9. Simulations: 64 globally coupled smooth oscillators. (a) The mean order parameter as a function of the coupling strength at $V = 4.5$, $R0 = 5.4$, $\gamma = 0.5$, and $K_c = 0.021$. (b) Dependence of $1/(1 - \langle r'\rangle^2)$ on the coupling strength at different simulation conditions. Triangles: $V = 5$, $R0 = 5.4$, $\gamma = 0.5$, and $K_c = 0.0128$. Squares: $V = 4.5$, $R0 = 5.4$, $\gamma = 0.5$, and $K_c = 0.021$. Circles: $V = 4$, $R0 = 5.4$, $\gamma = 0.5$, and $K_c = 0.0315$. Dashed line: $1/(1 - \langle r'\rangle^2) = 1$. (c) Variance of the order parameter as a function of K under the same simulation conditions as those of part a. (d) Variance of the order parameter as a function of K at $V = 5$, $R0 = 5.4$, $\gamma = 0.5$, and $K_c = 0.0128$.

oscillators is smaller, the two-step character of the transition is less obvious, although there is still a small second peak in the variance.

Array of 512 Elements. We carried out simulations with a population of 512 smooth oscillators to investigate the effects of finite size. The mean order parameters for arrays of 64 and 512 elements as a function of coupling strength are shown in Figure 10a. At $K = 0$, $\langle r\rangle$ is 0.038 and 0.11 for 512 and 64 oscillators, respectively. This relationship between the two values is in accordance with a $N^{-1/2}$ scaling, $1/\sqrt{512} = 0.044$ and $1/\sqrt{64} = 0.125$. The increase in system size produces a flatter plateau below the critical coupling strength and a sharper transition at the critical point. At large coupling strengths, similar values of order are obtained for the two array sizes. The fits for the two array sizes (circles in Figure 10b) give a value of $K_c = 0.021$ for the conditions shown in Figure 10a. The rescaled plots are also shown (squares) for another set of conditions at which K_c is smaller. The variance of order for these two conditions is shown in Figure 10c,d. The variance decreases with increasing array size, in accordance with the theoretical work of Daido,[23] and the multipeak character around the critical coupling strength is less evident for the larger array.

Gaussian Frequency Distribution. We carried out simulations with a Gaussian frequency distribution to explore the effects of the explicit form of the distribution. Parts a and b of Figure 11 are frequency histograms for uncoupled 64 oscillators constructed with Lorentzian and Gaussian distributions in the heterogeneity parameter Δ_k, respectively. They have the same mean frequency of 0.0842 and a standard derivation of 5.5×10^{-4}. The Gaussian distribution has fewer elements both at (about half as many) and far from the mean frequency. In Figure 11c the mean order parameter is shown as a function of the coupling strength for the two distributions. The critical coupling strength for the Gaussian distribution ($K_c = 0.05$) is over twice that for the Lorentzian distribution ($K_c = 0.02$). This is consis-

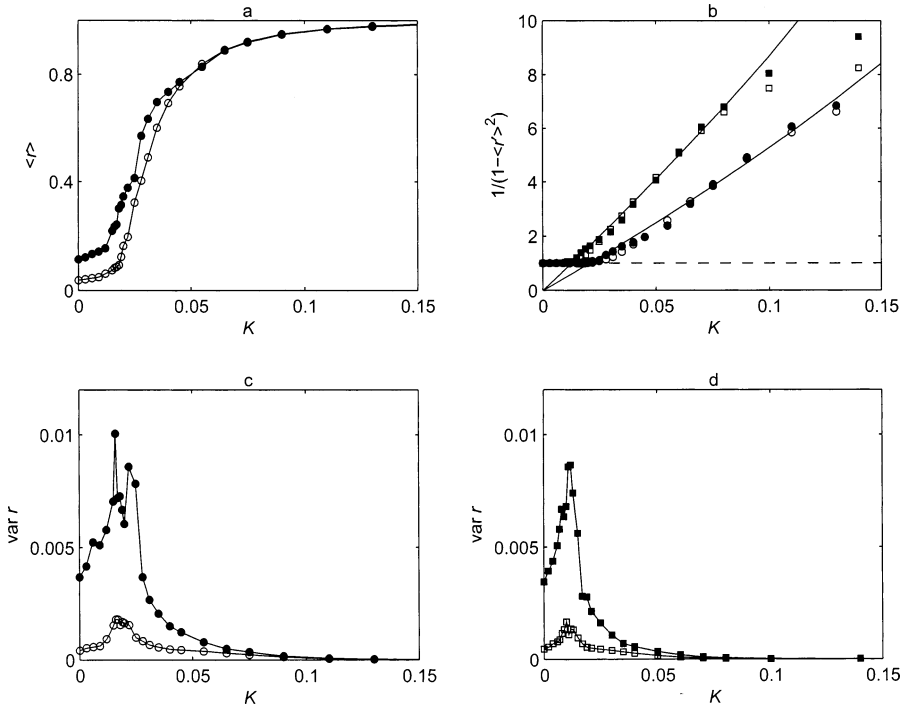

Figure 10. Simulations: comparison of 64 and 512 globally coupled smooth oscillators. Solid symbols: $N = 64$. Open symbols: $N = 512$. (a) The mean order parameter as a function of the coupling strength at $V = 4.5$, $R0 = 5.4$, $\gamma = 0.5$, and $K_c = 0.021$. (b) Dependence of $1/(1 - \langle r' \rangle^2)$ on the coupling strength at different simulation conditions. Solid and open circles, for the case of $V = 4.5$ as described in part a. Solid and open squares, $V = 5$, $R0 = 5.4$, $\gamma = 0.5$, and $K_c = 0.0128$. (c) Variance of the order parameter as a function of K under the same simulation conditions as those in part a. (d) Variance of the order parameter as a function of K for the case of $V = 5$ as described in part b.

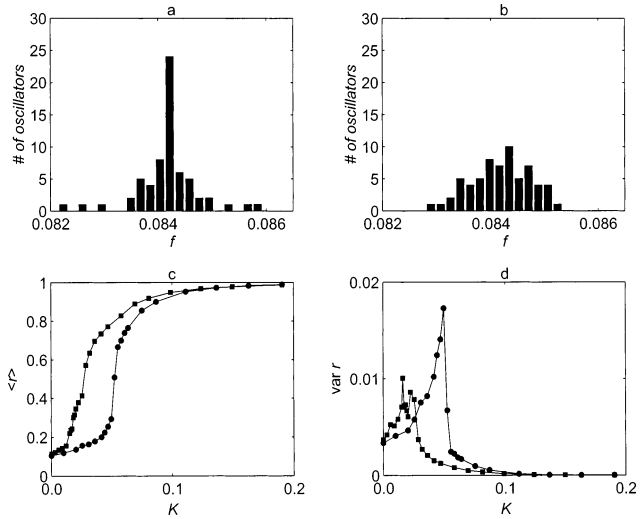

Figure 11. Simulations: comparison of 64 globally coupled smooth oscillators with Lorentzian and Gaussian distributions in Δ_k. (a) Histogram of intrinsic frequencies with Lorentzian distribution. $V = 4.5$, $R0 = 5.4$, and $\gamma = 0.5$. (b) Histogram of intrinsic frequencies with Guassian distribution. $V = 4.5$, $R0 = 5.4$, and $\sigma = 0.7$. (c) The mean order parameter as a function of the coupling strength. Squares: Lorentzian distribution with the same conditions as those in part a, where $K_c = 0.021$. Circles: Gaussian distribution with the same conditions as those in part b, where $K_c = 0.050$. (d) Variance of the order parameter as a function of K, with the same representations of symbols as those in part c.

tent with Kuramoto's theory[1] that predicts that the critical coupling strength is inversely proportional to the fraction of oscillators at the peak frequency. Above the critical coupling strength, the order rises; for the Gaussian case, the rise is steeper and the (single-peak) maximum in the variance is larger (Figure 11d).

C. Populations of Relaxation Oscillators. The relaxation character of the oscillations varies with the distance from the saddle-loop bifurcation. The saddle-loop bifurcation takes place at about $V = 26.5$ with $R0 = 20$ (Figure 7). Below $V = 24$, the synchronization properties are very similar to those with smooth oscillators. Above $V = 24$, differences start to occur. We consider here $V = 24.5$, which yields the relaxation oscillators seen in Figure 7e,f.

The effects of coupling strength on the behavior of a population of 64 relaxation oscillators are shown in Figure 12. The figure can be compared to Figure 8 for smooth oscillators; i.e., both figures show frequency distributions, frequency against inherent frequency, and the order parameter for $K = 0$ and for two small nonzero values of K. Partial synchronization can be seen at $K = 0.0989$ (Figure 12b,e); although only two elements are synchronized, the other elements are also affected. All frequencies shift to higher values, and this effect is greater than that observed with the smooth oscillators. The slope of $f_j(K)$ vs $f_j(K=0)$ is less than 1 for most of the range. The effect of added coupling is felt more strongly by the oscillators of lower frequency and the synchronization occurs for these values; this was also seen in the experiments (Figure 5e). There is also a larger variation of $r(t)$ than for the smooth oscillators. For $K = 1.5$ (last column of Figure 12), the oscillators are almost synchronized (at a frequency slightly larger than the mean frequency) and the order is almost 1 with a very small variance. With a further increase of the coupling strength, the synchronized frequencies approach the mean intrinsic frequency.

A sharp transition in the mean order is seen in Figure 13a at about $K_c = 0.0989$. The strong enhancement of

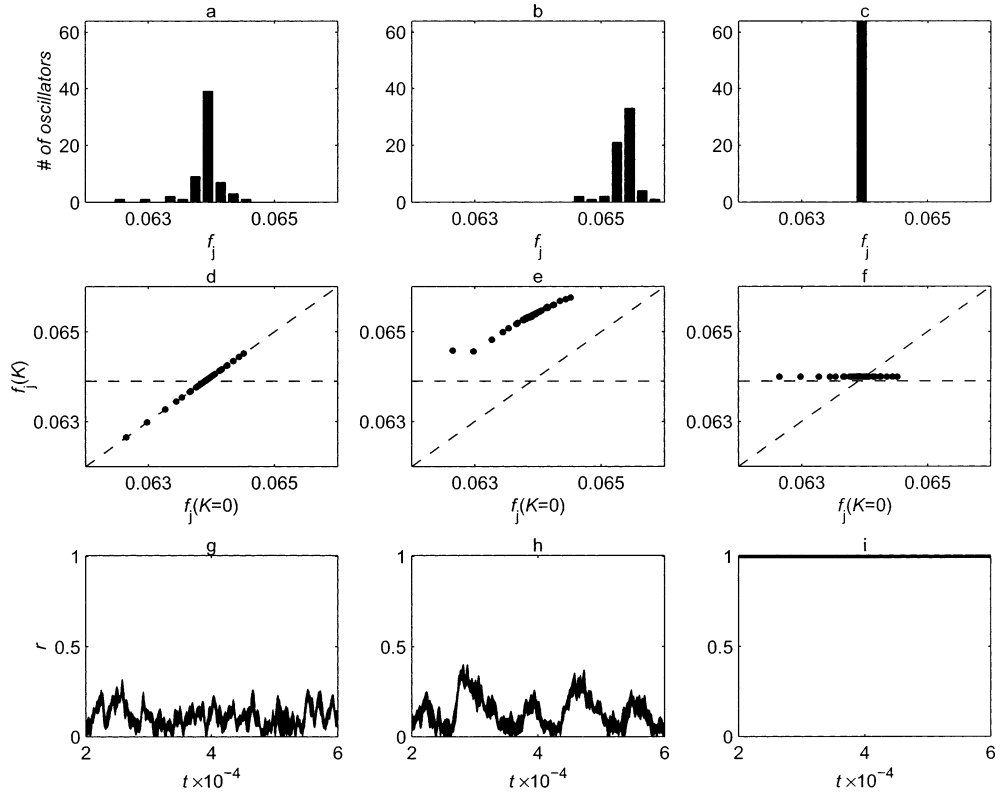

Figure 12. Simulations: 64 globally coupled relaxation oscillators at $V = 24.5$, $R0 = 20$, $\gamma = 0.2$, and $K_c = 0.0989$. Left column: $K = 0$. Middle column: $K = 0.0989$. Right column: $K = 1.5$. Top row: histograms of the frequencies f_j. Middle row: frequencies at different coupling strengths $f_j(K)$ versus the corresponding frequencies without coupling ($K = 0$). Bottom row: time series of the order parameter.

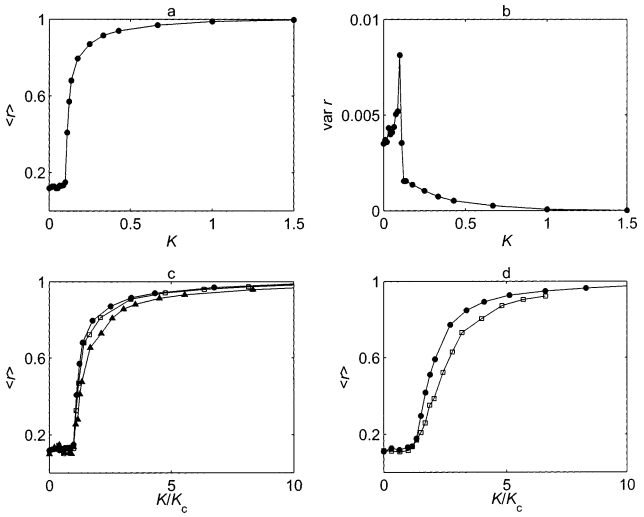

Figure 13. Simulations: 64 globally coupled relaxation oscillators. (a) The mean order parameter as a function of the coupling strength. $V = 24.5$, $R0 = 20$, $\gamma = 0.2$, and $K_c = 0.0989$. (b) Variance of the order parameter as a function of K, with the same conditions as those in part a. (c) The mean order parameter as a function of K/K_c for sets of coupled relaxation oscillators at $V = 24.5$ and $R0 = 20$. Solid circles: $\gamma = 0.2$ and $K_c = 0.0989$. Open squares: $\gamma = 0.1$ and $K_c = 0.0526$. Solid triangles: $\gamma = 0.05$ and $K_c = 0.0246$. (d) The mean order parameter as a function of K/K_c for sets of coupled relaxation oscillators at $V = 24.8$ and $R0 = 20$. Solid circles: $\gamma = 0.1$ and $K_c = 0.065$. Open squares: $\gamma = 0.05$ and $K_c = 0.031$.

the fluctuations of order occurs in a small region of coupling strength around K_c.

We explored the dependency on the parameters V (applied potential) and γ (width of the frequency distribution), as shown in Figure 13c,d. The mean order is shown in Figure 13c at a fixed V for three values of γ. With increasing γ, the critical coupling strength K_c increases and the dependence of $\langle r \rangle$ on K/K_c is steeper. Recent theoretical results[24] on infinite-size systems predict a transition (depending on the nature of the relaxation oscillator) that is either less steep than the smooth behavior or discontinuous with hysteresis. Hysteresis was not found in any of simulations, and the very steep behavior appears to be continuous. Thus, a complete understanding of the steep increase in order seen in both the experiments and the simulations is not yet available. At a potential closer to the saddle-loop bifurcation, Figure 13d, similar trends are seen but the dependence of $\langle r \rangle$ on K/K_c is less steep. (The closer to the saddle-loop bifurcation the oscillations are, the more relaxational they are and longer their period, and thus a population of oscillators has a greater degree of heterogeneity.)

At circuit potentials even larger than that of Figure 13d, very close to the saddle-loop bifurcation, the relaxation oscillators do not synchronize at weak coupling. With stronger coupling ($K > 0.5$), amplitude clustering along with a change in the waveform of the oscillators is observed.

Concluding Remarks

Reaction sites for surface reactions are typically heterogeneous or nonidentical. The individual elements of the array of electrodes used in this study vary because of several factors. The sizes and compositions of the metal vary slightly, and polishing results in a nonuniform roughness. Small differences occur in the thicknesses and compositions of nickel oxide and hydroxide films that build up during the reaction. The mass

transfer coefficient varies somewhat over the surface. There is also a current distribution in electrochemical reactions, and so the edge elements on 8 × 8 arrays of electrodes have a somewhat higher current.[45] Although all of these effects are small, they do produce a measurable difference among the elements. In the oscillatory region, there is a frequency distribution of the oscillators. Such heterogeneities are found in almost all experimental systems consisting of an ensemble of elements.

The applicability of the theories on synchronization of populations of ideal oscillators to multivariable nonideal systems in laboratory experiments or in other chemical, biological, or engineering applications had not been well explored. We used the metal dissolution as a model system for verifying the theories on heterogeneous oscillators. The electrodissolution of Ni exhibits well-controllable and easily measurable oscillatory dynamics. The array of 64 elements is large enough to obtain information on theoretical predictions and also gives an insight on finite-size effects. In the experiments the critical coupling threshold K_c, at which oscillators with inherent frequencies near the mean become synchronized, was seen. The experiments with smooth oscillators were done under varying conditions such that the amplitude of oscillations and the width of the frequency distribution changed, but the shape of the frequency distribution remained approximately fixed. The mean order $\langle r \rangle$ depended on the parameter K/K_c in accordance with the analytical prediction.[1]

With changing experimental conditions (the circuit potential and total external resistance), relaxation oscillators were obtained. The frequency distribution of the relaxation oscillators is wider and flatter than that of the smooth oscillators. Therefore, aggregate effects of both of these factors are seen. For relaxation oscillators, the critical coupling point is larger, and above it, the dependence of order on the coupling strength is typically steeper than that of smooth oscillators. Asymmetries in the synchronization process were seen; slower oscillators are easier to entrain, and the system has a tendency to synchronize to a higher frequency than the inherent mean frequency.

Near the critical coupling strength, the variance of the order has a maximum for both types of oscillators. The order fluctuations are larger for the relaxation oscillators.

Numerical simulations showed that some aspects of the theories on ideal, infinite-size populations of oscillators can be used to interpret emerging coherence in nonideal, finite-size systems. The model reproduces many features of the experiments. It shows a critical point for synchronization and enhanced fluctuations of order for both smooth and relaxation oscillators; it exhibits asymmetric synchronization of relaxation oscillators and increased entrained frequencies. Some finite-size-related effects were identified; with wider frequency distribution populations, the transition consisted of two steps in which oscillators with lower, and then higher, frequencies are synchronized. The numerical simulations verified the experimental observation that the frequency of the synchronized oscillators can be greater than the mean of the inherent frequencies and that this tendency becomes stronger as the relaxational character of the oscillators is increased. Similar phenomena have been explored in previous theoretical[20] and numerical[46] studies.

In both simulations and experiments with relaxation oscillators, the transition to synchronization can occur in a very narrow range of coupling strength without hysteresis.

The experiments and simulations with the electrochemical system show that the nature of the onset of synchronization predicted by the theoretical studies of Winfree and Kuramoto is found also in nonideal systems of finite size. Similar emergence of coherence should be found generally in a variety of chemical, biological, ecological, and engineering systems in which heterogeneous cyclic elements interact.

Acknowledgment

We thank Reuel Shinnar for many years of friendship, inspiration, and fascinating conversations. This work was supported by the National Science Foundation (Grant CTS-0000483) and the Office of Naval Research (Grant N00014-01-1-0603).

Literature Cited

(1) Kuramoto, Y. *Chemical oscillations, waves and turbulence*; Springer: Berlin, 1984.

(2) Mertens, F.; Imbihl, R.; Mikhailov, A. Breakdown of global coupling in oscillatory chemical-reactions. *J. Chem. Phys.* **1993**, *99*, 8668.

(3) Slinko, M. M.; Ukharskii, A. A.; Jaeger, N. I. Global and non-local coupling in oscillating heterogeneous catalytic reactions: The oxidation of CO on zeolite supported palladium. *Phys. Chem. Chem. Phys.* **2001**, *3*, 1015.

(4) Middya, U.; Luss, D. Impact of global interactions on patterns in a simple system. *J. Chem. Phys.* **1994**, *100*, 6386.

(5) Lobban, L.; Luss, D. Spatial Temperature Oscillations During Hydrogen Oxidation on a Nickel Foil. *J. Phys. Chem.* **1989**, *93*, 6530.

(6) Krischer, K. In *Modern Aspects of Electrochemistry*; Conway, B. E., Bockris, O. M., White, R. E., Eds.; Kluwer Academic/Plenum Press: New York, 1999; Vol. 32, p 1.

(7) Mazouz, N.; Flätgen, G.; Krischer, K. Tuning the range of spatial coupling in electrochemical systems: From local via nonlocal to global coupling. *Phys. Rev. E* **1997**, *55*, 2260.

(8) Mazouz, N.; Flätgen, G.; Krischer, K.; Kevrekidis, I. G. The impact of the operation mode on pattern formation in electrode reactions—From potentiostatic to galvanostatic control. *J. Electrochem. Soc.* **1998**, *145*, 2404.

(9) Otterstedt, R. D.; Jaeger, N. I.; Plath, P. J.; Hudson, J. L. Global coupling effects on spatiotemporal patterns on a ring electrode. *Chem. Eng. Sci.* **1999**, *54*, 1221.

(10) Bär, M.; Hildebrand, M.; Eiswirth, M.; Falcke, M.; Engel, H.; Neufeld, M. Chemical Turbulence and Standing Waves in a Surface Reaction Model: The Influence of Global Coupling and Wave Instabilities. *Chaos* **1994**, *4*, 499.

(11) Middya, U.; Luss, D.; Sheintuch, M. Spatiotemporal Motions Due to Global Interaction. *J. Chem. Phys.* **1994**, *100*, 3568.

(12) Kiss, I. Z.; Wang, W.; Hudson, J. L. Experiments on arrays of globally coupled periodic electrochemical oscillators. *J. Phys. Chem. B* **1999**, *103*, 11433.

(13) Wang, W.; Kiss, I. Z.; Hudson, J. L. Experiments on arrays of globally coupled chaotic electrochemical oscillators: synchronization and clustering. *Chaos* **2000**, *10*, 248.

(14) Liauw, M. A.; Plath, P. J.; Jaeger, N. I. Complex oscillations and global coupling during the catalytic oxidation of CO. *J. Chem. Phys.* **1996**, *104*, 6375.

(15) Liauw, M. A.; Ning, J.; Luss, D. Pattern formation on a nonuniformly active ring. *J. Chem. Phys.* **1996**, *104*, 5657.

(16) Winfree, A. T. *The geometry of biological time*; Springer-Verlag: New York, 1980.

(17) Kiss, I. Z.; Zhai, Y.; Hudson, J. L. Collective dynamics of a weakly coupled electrochemical reaction on an array. *Ind. Eng. Chem. Res.* **2002**, *41*, 6363.

(18) Kiss, I. Z.; Zhai, Y.; Hudson, J. L. Collective dynamics of chaotic chemical oscillators and the law of large numbers. *Phys. Rev. Lett.* **2002**, *88*, 238301.

(19) Slinko, M. M.; Ukharskii, A. A.; Peskov, N. V.; Jaeger, N. I. Chaos and synchronisation in heterogeneous catalytic systems: CO oxidation over Pd zeolite catalysts. *Catal. Today* **2001**, *70*, 341.

(20) Winfree, A. T. Biological Rhythms and the Behavior of Populations of Coupled Oscillators. *J. Theor. Biol.* **1967**, *16*, 15.

(21) Kuramoto, Y. Cooperative Dynamics of Oscillator Community. *Prog. Theor. Phys. Suppl.* **1984**, *79*, 223.

(22) Kuramoto, Y. In *International Symposium on Mathematical Problems in Theoretical Physics, Lecture Notes in Physics*; Araki, H., Ed.; Springer: New York, 1975; Vol. 39, p 420.

(23) Daido, H. Intrinsic Fluctuation and Its Critical Scaling in a Class of Populations of Oscillators With Distributed Frequencies. *Prog. Theor. Phys.* **1989**, *81*, 727.

(24) Daido, H. Onset of cooperative entrainment in limit-cycle oscillators with uniform all-to-all interactions: Bifurcation of the order function. *Physica D* **1996**, *91*, 24.

(25) Mirollo, R. E.; Strogatz, S. H. Synchronization of Pulse-Coupled Biological Oscillators. *SIAM J. Appl. Math.* **1990**, *50*, 1645.

(26) Strogatz, S. H. From Kuramoto to Crawford: exploring the onset of synchronization in populations of coupled oscillators. *Physica D* **2000**, *143*, 1.

(27) York, R. A.; Compton, R. C. Quasi-Optical Power Combining Using Mutually Synchronized Oscillator Arrays. *IEEE Trans. Microwave Theory Tech.* **1991**, *39*, 1000.

(28) Oliva, R. A.; Strogatz, S. H. Dynamics of a large array of globally coupled lasers with distributed frequencies. *Int. J. Bifurcation Chaos* **2001**, *11*, 2359.

(29) Wiesenfeld, K.; Colet, P.; Strogatz, S. H. Synchronization transitions in a disordered Josephson series array. *Phys. Rev. Lett.* **1996**, *76*, 404.

(30) Walker, T. J. Acoustic Synchrony: Two Mechanisms in the Snowy Tree Cricket. *Science* **1969**, *166*, 891.

(31) Buck, J. Synchronous Rhythmic Flashing of Fireflies. II. *Q. Rev. Biol.* **1988**, *63*, 265.

(32) Néda, Z.; Ravasz, E.; Brechet, Y.; Vicsek, T.; Barabási, A. L. The sound of many hands clapping—Tumultuous applause can transform itself into waves of synchronized clapping. *Nature* **2000**, *403*, 849.

(33) Ghosh, A. K.; Chance, B.; Pye, E. K. Metabolic Coupling and Synchronization of NADH Oscillations in Yeast Cell Populations. *Arch. Biochem. Biophys.* **1971**, *145*, 319.

(34) Danø, S.; Sørensen, P. G.; Hynne, F. Sustained oscillations in living cells. *Nature* **1999**, *402*, 320.

(35) Danø, S.; Hynne, F.; De Monte, S.; d'Ovidio, F.; Sørensen, P. G.; Westerhoff, H. Synchronization of glycolytic oscillations in a yeast cell population. *Faraday Discuss.* **2001**, *120*, 261.

(36) Wiener, N. *Nonlinear Problems in Random Theory*; MIT Press: Cambridge, MA, 1958.

(37) Michaels, D. C.; Matyas, E. P.; Jalife, J. Mechanisms of Sinoatrial Pacemaker Synchronization: A New Hypothesis. *Circ. Res.* **1987**, *61*, 704.

(38) Winfree, A. T. On emerging coherence. *Science* **2002**, *298*, 2336.

(39) Kiss, I. Z.; Zhai, Y. M.; Hudson, J. L. Emerging coherence in a population of chemical oscillators. *Science* **2002**, *296*, 1676.

(40) Lev, O.; Wolffberg, A.; Sheintuch, M.; Pismen, L. M. Bifurcations to Periodic and Chaotic Motions in Anodic Nickel Dissolution. *Chem. Eng. Sci.* **1988**, *43*, 1339.

(41) Pikovsky, A. S.; Rosenblum, M. G.; Osipov, G. V.; Kurths, J. Phase synchronization of chaotic oscillators by external driving. *Physica D* **1997**, *104*, 219.

(42) Gábor, D. *J. Inst. Electr. Eng., Part 3* **1946**, *93*, 429.

(43) Haim, D.; Lev, O.; Pismen, L. M.; Sheintuch, M. Modeling Periodic and Chaotic Dynamics in Anodic Nickel Dissolution. *J. Phys. Chem.* **1992**, *96*, 2676.

(44) Wang, W. Synchronization and Clustering of Arrays of Electrochemical Oscillators. Ph.D. Thesis, University of Virginia, Charlottesville, Virginia, 2001.

(45) Newman, J. *Electrochemical Systems*; Prentice Hall: Engelwood Cliffs, NJ, 1973.

(46) Sakaguchi, H.; Kuramoto, Y. A soluble active rotator model showing phase transition via mutual entrainment. *Prog. Theor. Phys.* **1986**, *76*, 576.

Received for review February 20, 2003
Revised manuscript received May 15, 2003
Accepted May 16, 2003

IE030164Z